Biosensors and Bioelectronics 142 (2019) 111558

Contents lists available at ScienceDirect

Biosensors and Bioelectronics

journal homepage: www.elsevier.com/locate/bios

An electrochemical biosensor integrating immunoassay and enzyme activity analysis for accurate detection of active human apurinic/apyrimidinic endonuclease 1

Mengru Zhou[a,1], Chang Feng[a,b,1], Dongsheng Mao[a], Shiqi Yang[a], Lingjie Ren[a], Guifang Chen[a,*], Xiaoli Zhu[a,**]

[a] Center for Molecular Recognition and Biosensing, School of Life Sciences, Shanghai University, Shanghai, 200444, PR China
[b] State Key Laboratory of Pharmaceutical Biotechnology and Collaborative Innovation Center of Chemistry for Life Sciences, Department of Biochemistry, Nanjing University, Nanjing, 210093, PR China

ARTICLE INFO

Keywords:
Human apurinic/apyrimidinic endonuclease 1
Electrochemical detection
Immunoassay
Enzyme activity analysis
Catalytic hairpin assembly

ABSTRACT

A novel electrochemical biosensing method that can take into account both immunoassay and enzyme activity analysis was reported in this work for determination of the enzymatically active human apurinic/apyrimidinic endonuclease 1 (APE1). The basic principle is to design and construct a DNA catalytic hairpin assembly (CHA) triggered by APE1 catalysis in enzyme activity analysis, and the assembled DNAs are labeled with electrochemically active CdS and PbS quantum dots to output electrochemical signals. In this system, the signal generation needs to satisfy both the conditions of immunological recognition and enzymatic catalysis, providing a basis for accurate analysis of active APE1. Results show that this method can reflect the regulation of the enzyme activity and can also distinguish APE1 from its isozymes with the same enzyme activity. The concept and successful implementation of this integrated system will contribute to the research and application of APE1 in biomedicine, and provide a reference for the accurate analysis of other enzymes.

1. Introduction

Human apurinic/apyrimidinic endonuclease 1 (APE1), also known as redox effect factor 1 (Ref1), is an intracellular multifunctional enzyme (Antoniali et al., 2017; Gerhard and Bernd, 1999). It plays an important role in oxidative stress response and regulation of transcription factors and cell cycle (Lipton et al., 2008). In addition, a key function of APE1 is base excision repair (BER) with a mechanism as following (Katarzyna et al., 2001; Demple and Sung, 2005): Firstly, the removal of DNA base lesion process is mediated by ROS and monofunctional DNA glycosylases to form apurinic/apyrimidinic (AP) site. APE1 recognizes and cuts the AP site in double-stranded DNA, producing 3′ OH and 5′ deoxyribose phosphate (5′ dRP) end. Then DNA polymerase β (Polβ) with intrinsic 5′ dRP lyase activity removes dRP residue to create a linkable 5′ P terminus and also incorporates the missing nucleotide (nt) at the 3′ OH terminus. The resulting nick is sealed by DNA ligase to complete single nucleotide incorporation (Hegde et al., 2008; Hegde et al., 2012; Whitaker et al., 2018). BER has been considered to be one of the mechanisms of tumorigenesis, and APE1 is observed to be highly expressed in tumor cells (Pascut et al., 2019; Wang et al., 2019). Therefore, the quantitative detection of APE1 is critical for the screening and treatment of cancers. Various methods have been developed, which can be classified into two categories: immunoassay and enzyme activity analysis. For the former, typical methods include Western blotting, enzyme-linked immunosorbent assay (ELISA) and electrochemical immunosensors (Chang et al., 2013; Shin et al., 2015; Zhuo et al., 2014; Zhong et al., 2014; Zhao et al., 2014; Han et al., 2013). And for the latter, DNA probes-assisted fluorescence spectrometry is usually adopted (Fang et al., 2015; Gines et al., 2014).

Despite the successful application of these detection methods for the analysis of APE1, a dilemma exists and plagues researchers: the results of immunoassay methods can only show whether APE1 is present, but cannot show whether the APE1 is active. In some cases, e.g. the presence of inhibitors, the APE1 has lost its enzyme activity, but cannot be observed from the immunoassay results (Zhuo et al., 2014). This

* Corresponding author.
** Corresponding author.
E-mail addresses: gfchen@shu.edu.cn (G. Chen), xiaolizhu@shu.edu.cn (X. Zhu).
[1] Both authors contributed equally to this work.

https://doi.org/10.1016/j.bios.2019.111558
Received 14 June 2019; Received in revised form 21 July 2019; Accepted 31 July 2019
Available online 01 August 2019
0956-5663/

problem can be overcome by using enzyme activity analysis, which however brings a new problem: there are some isozymes of APE1 that have the same enzyme activity, e.g. endonuclease IV (Endo IV) and 8-oxoguanine DNA glycosylase (hOGG1) (Tsutakawa et al., 2013; Chaim et al., 2017). Enzyme activity analysis cannot distinguish whether the enzyme activity is from APE1 or its isozymes. This problem can be just solved by immunoassay. So in a word, immunoassay and enzyme activity analysis are complementary in the analysis of APE1. But it is a tedious work to analyze APE1 separately by two kinds of methods. And it is inconvenient for pooled analysis of the data from both sides. Biases of the results may also exist during the analysis. To integrate them each into a single system would contribute to an easily-operated assay and would make accurate analysis of active APE1 possible. Here, we report an integrated electrochemical biosensing system that gives consideration to both immunoassay and enzyme activity analysis. Though electrochemical techniques have been widely reported for enzyme biosensing using surface enzyme modification (McKenzie et al., 2013), the integration can provide accurate signals especially in the presence of target analogues.

2. Experimental section

2.1. Reagents and apparatuses

The DNA oligonucleotides (Hairpin I: 5′-TCAACATCAGTCTGATAA GCTACC

ATGTGTAGATAGCTTATCXCGCTGATGTTGA-3′; Hairpin II: 5′-TAAGCTATCT
ACACATGGTAGCTTATCAGACTCCATGTGTAGA-3′; Trigger chain: 5′-TAGCTT
ATCAGACTGATGT-3′; FAM-Probe: 5′- TGAAGAXTTCCTCCTTTTT-TAGGAGG

AATTCTTCATTTTT-3′, “X” as shown in red represents AP site) were purified by Sangon Biotechnology Co., Ltd. (Shanghai, China). Hairpin I/II whose terminals are modified with fluorophores or biotin are synthesized by Sangon Biotechnology Co., Ltd. Apurinic/apyrimidinic endonuclease (APE1) and endonuclease IV were purchased from TaKaRa (Dalian, China). Apurinic/apyrimidinic endonuclease antibody (anti-APE1, monoclonal antibody) was purchased from Santa Cruz Biotechnology, Inc. (U.S.A.). *para*-Sulfonatocalix[4]arene (pSC_4) was obtained from Tokyo Chemical Industry Co., Ltd. (Shanghai, China). Biotin and streptavidin were purchased from Sinopharm Chemical Reagent Co., Ltd. (Shanghai, China). Lead sulfide quantum dots (PbS QDs) were purchased from XingShuo Nanotechnology Co., Ltd. (Suzhou, China). Mercaptopropionic acid (MPA), sulfosuccinimidyl 4-(N-maleimidomethyl) cyclohexane-1-1-carboxylate (Sulfo-SMCC), N-(3-(dimethylamino)propyl)-N′-ethylcarbodiimide (EDC) and N-hydroxysuccinimide (NHS) were all purchased from Sigma-Aldrich. Cadmium chloride hydrate ($CdCl_2$) was purchased from Alfa Aesar Chemical Co., Ltd. (China). APE1 enzyme ELISA kit and native lysis buffer were purchased from Abcam (Shanghai, China).

2.2. Synthesis of cadmium sulfide quantum dots (CdS QDs)

CdS QDs were synthesized according to our previous reports (Li et al., 2010). Briefly, 100 mL deionized water was firstly deoxygenated by bubbling nitrogen for 1 h. Then $CdCl_2$ (1 mM) and MPA (2.4 mM) were added into the aqueous solution, the pH of which was adjusted to 8.0–8.5 with 1 M NaOH solution. Nitrogen was further bubbled through the solution for another 30 min. Next, 0.625 mM thioacetamide was added into the above $CdCl_2$-MPA solution and the final molar ratio of Cd^{2+}/MPA/S^{2-} in the solution was 1:2.4:0.625. The resulting mixture solution was reacted at 100 °C and stirred vigorously for 10 h away from light, which gradually turned pale yellow. Subsequently, the solution was cooled to room temperature slowly and ultrafiltered to remove excessive MPA by using Vivaspin 500 (50,000 MW) at 5000 rpm for 20 min at 4 °C. After washing twice, the CdS quantum dots purified and concentrated with an ultrafiltration centrifuge tube were dissolved in PBS solution at pH 7.4, and stored at 4 °C until use.

2.3. Construction of APE1-activated DNA catalytic hairpin assembly

The hairpin I and hairpin II were diluted to 10 μM using buffer 1.1 (10 mM Bis-Tris Propane-HCl, 10 mM $MgCl_2$, 100 g/mL BSA, pH 7.9) and kept at 95 °C for 5 min. Then the solution was cooled to room temperature slowly. 500 nM hairpin I was incubated with different concentration of APE1 (0–5 U/mL) containing buffer 1.1 at 37 °C for 30 min. Next, 500 nM trigger chain and 500 nM hairpin II were added into the above solution and the mixture was incubated at 37 °C for 2 h to perform DNA catalytic hairpin assembly.

2.4. Electrophoresis analysis and fluorescence measurements

To verify the feasibility of DNA catalytic hairpin assembly triggered by APE1 catalysis, the reaction products were analyzed on electrophoresis system. A 20% nondenaturating polyacrylamide gel loaded with 10 μL samples was run in 1 × Tris boric acid EDTA (TBE) for 90 min at 120 V, then followed the staining of SYBR I for 30 min. Imaging of the gel was performed using the Gel Doc XR Imaging System (Bio-Rad, USA). Fluorescence analysis was adopted by a HitachiF-7000 fluorescence spectrophotometer (Tokyo, Japan). The emission spectra were recorded at a scan rate of 2 nm/s with an excitation intensity of 494 nm and 650 nm, and the fluorescence intensity at 520 nm and 670 nm was recorded for FAM and Cy5, respectively.

2.5. Conjugation of quantum dots on hairpin I/II

The MPA-COOH modified CdS QDs were activated by EDC-NHS (Huang et al., 2000; Li et al., 2016). Briefly, EDC (15 mM) and NHS (75 mM) were added into the solution containing COOH–CdS (1 mM) and incubated at 37 °C for 0.5–1 h. Then 500 nM hairpin I modified with NH_2 was added to the activated CdS QDs. Subsequently, the reaction was carried out at 37 °C for 2 h and hairpin I modified with CdS QDs was obtained successfully. The hairpin II with NH_2 attached to the end was modified with PbS QDs encapsulated by MPA-COOH in the same method.

2.6. APE1-triggered catalyzed hairpin assembly

The CdS QDs and biotin modified hairpin I (500 nM) was dissolved in buffer 1.1 and was incubated with different concentration of APE1 at 37 °C for 30 min. Then, 500 nM trigger chain and 500 nM PbS QDs modified hairpin II were added into the CHA reaction system at 37 °C for 2 h.

2.7. Electrode interface modification and immuno-assembly

1 mM pSC_4 was immobilized on the clean bare gold electrode via the coordinate bond between the gold atoms on the surface of gold electrode and the “-SO_3^- group” of pSC_4 after 6 h of incubation at room temperature (Dong et al., 2018; Wang et al., 2018). Unbound pSC_4 was washed off by rinsing the electrodes with doubly distilled water. Then anti-APE1 antibody (Ab1) at a concentration of 1.0×10^{-5} M was immobilized onto the modified electrode through host-guest recognition of Fc region binding to pSC_4 (Chen et al., 2010; Lee et al., 2003). After incubation at 4 °C overnight, the modified electrode was extensively rinsed with double distilled water to remove excess unbound antibody. Sulfo-SMCC was used to generate a stable maleimide-activated antibody (Ab2) that is reactive with sulfhydryl groups generated in biotin (Zhao et al., 2010). The product of section 2.6, containing the

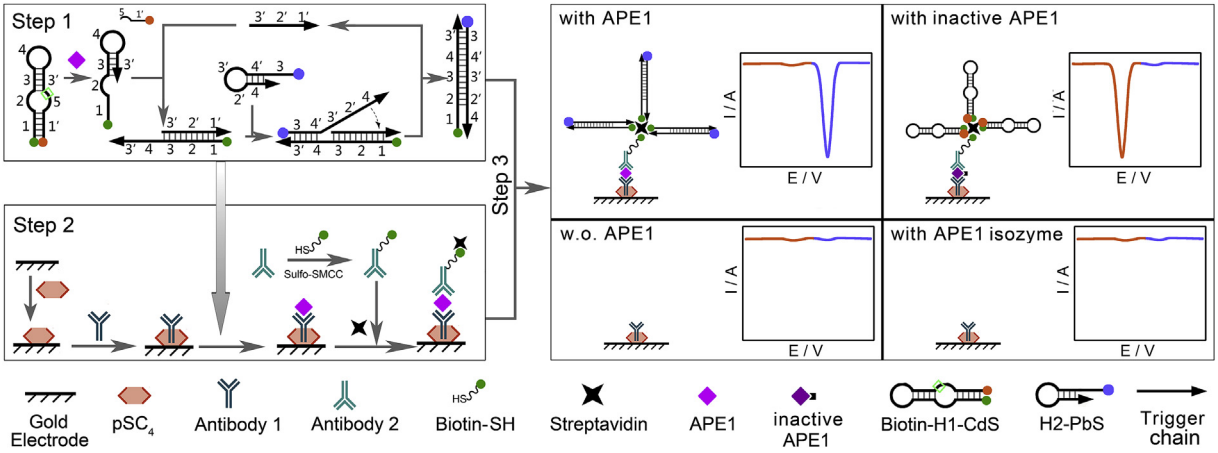

Scheme 1. Principle of the integrated electrochemical system for the accurate detection of APE1. H1: hairpin I, H2: hairpin II.

target APE1 as well as the CHA product, was incubated with the Ab1-functionalized electrode for 1 h to allow the capture of the APE1 onto the electrode. The supernatant solution was removed and kept for further usage, whereas the electrode was further incubated with Ab2 and streptavidin successively for 1 h each. Finally, the kept solution containing the CHA product, was incubated with the electrode for another 1 h. As a result, a structure of pSC_4/Ab1/APE1/Ab2/DNA-QDs was obtained on the electrode. After every step, the modified electrode was extensively rinsed with double distilled water to prevent physical adsorption. The process of modification was characterized by electrochemical impedance spectroscopy (EIS) and cyclic voltammetry (CV), which was obtained with a 50 mM PBS (pH 7.0) buffer containing 5 mM $[Fe(CN)_6]^{3-/4-}$ as electrolyte. For EIS, the parameters used are as follows: the frequency range is from 0.1 Hz to 10 kHz and the alternative voltage is 5 mV. For CV, the parameters used are as follows: the potential is from −0.8 V to +0.8 V and the scan rate is 50 mV/s.

2.8. Anodic stripping voltammetry (ASV) for measuring signals

The above gold electrode of the modified pSC_4/Ab1/APE1/Ab2/DNA-QDs was immersed in 0.01 M HCl and 0.1 M HNO_3 for 1 h to dissolve the Pb^{2+} and Cd^{2+} signals, respectively. The resulting solution was then mixed with 5 mL 0.2 M pH 5.2 HAc-NaAc buffer for electrochemical analysis by using ASV technique with a mercury film modified glassy carbon electrode (Li et al., 2010; Qin et al., 2016). The polished glassy carbon electrode was inserted into 0.1 mol/L NH_4Cl solution containing 0.3 mM Hg^{2+} at −1.2 V for 300 s and the Hg^{2+} film modified glassy carbon electrode was obtained. The anodic stripping detection was carried out by first electrodeposition of cadmium at −1.1 V for 4 min and then stripping from −0.9 V to −0.2 V under N_2 atmosphere using a square-wave voltammetric waveform, with a 4 mV potential step, a 15 Hz frequency, and an amplitude of 25 mV. Before the measurement, the sodium acetate electrolyte was thoroughly deaerated by 15 min of nitrogen bubbling. Nitrogen gas was also gently blown into the liquid surface to ensure an oxygen-free environment, which avoids the interference of the electrochemical reduction of O_2 to the detection signals (Li et al., 2015; Sutter et al., 2004).

2.9. ELISA

In the conventional ELISA experiments, 50 μL volumes of serial dilutions of each test antigen were added to the capture antibody-coated well of the microplate. The microplate was incubated at 37 °C for 1 h and then washed three times. 100 μL of the horseradish peroxidase (HRP)-labeled detection antibody was added and incubated at 37 °C for 1 h with shaking. After washing, 100 μL of TMB substrate was added to each well and incubated for 10 min in the dark with shaking at 400 rpm. Then, 50 μL of stop solution was added to stop the reaction, and the plate was read using an ELISA plate reader at 450 nm. Blank and parallel groups should be set for each experiment.

2.10. Real sample detection

L02 (human normal liver cell line), HeLa (immortal cell line) and A549 (human lung cancer cell line) are adopted for real sample detection. These cells were cultured in RPMI 1640 or DMEM supplemented with 10% FBS. All cells were maintained in a humidified incubator at 37 °C with 5% CO_2 and 80% relative humidity. 1.0×10^3 cells were lysed on ice for 15 min with native lysis buffer. Next, the samples were centrifuged at 14,000 rpm at 4 °C for 15 min. Then, APE1 enzyme in the supernatant was detected by our method which have been described in the above steps.

3. Results and discussion

3.1. Principle

The principle of the integrated electrochemical system is shown in Scheme 1. First, an oligonucleotide (hairpin I) working as the substrate of both APE1 and CHA is elaborately designed. It contains two stem-loop structures and is labeled with biotin and CdS QDs at 5′-end and 3′-end respectively. At the middle loop, there is an AP site that can be recognized and cut by APE1. Once being cut, the 3′-end fragment with CdS QDs is released, leaving the 5′-end region exposed to work as a toehold to initiate CHA. The mechanism of CHA has been widely reported and will not be repeated here (He et al., 2019; Xiao et al., 2018). The only thing that should be noted is that the hairpin II is labeled with PbS QDs. After a cyclic CHA reaction, hybrid of cut hairpin I and hairpin II is produced, which contains a biotin and a PbS QD. In the meanwhile, a gold electrode is prepared, on which a sandwich of Ab1-APE1-Ab2 is fabricated in the presence of the target APE1. The upper antibody is biotin-labeled and can recruit the hybrid of I/II through streptavidin-biotin conjugation. Thereafter, the PbS QDs on the hybrid can work as an electrochemical probe for ASV analysis. In this scheme, the generation of ASV signals of PbS QDs needs to satisfy both the conditions of immunological recognition and enzymatic catalysis. In the absence of APE1 or in the presence of any other proteins that cannot be immunologically recognized (including isozymes), the hybrid of I/II cannot be recruited onto the surface of electrode, producing no electrochemical signals. And, in the case that the APE1 is immuno-active but catalysis-inactive, e.g. in the presence of inhibitors, the sandwich structure can still be fabricated, but recruit the intact hairpin I instead of the hybrid of I/II, outputting ASV signals of CdS QDs. In this way, accurate detection of enzymatically active APE1 can be achieved.

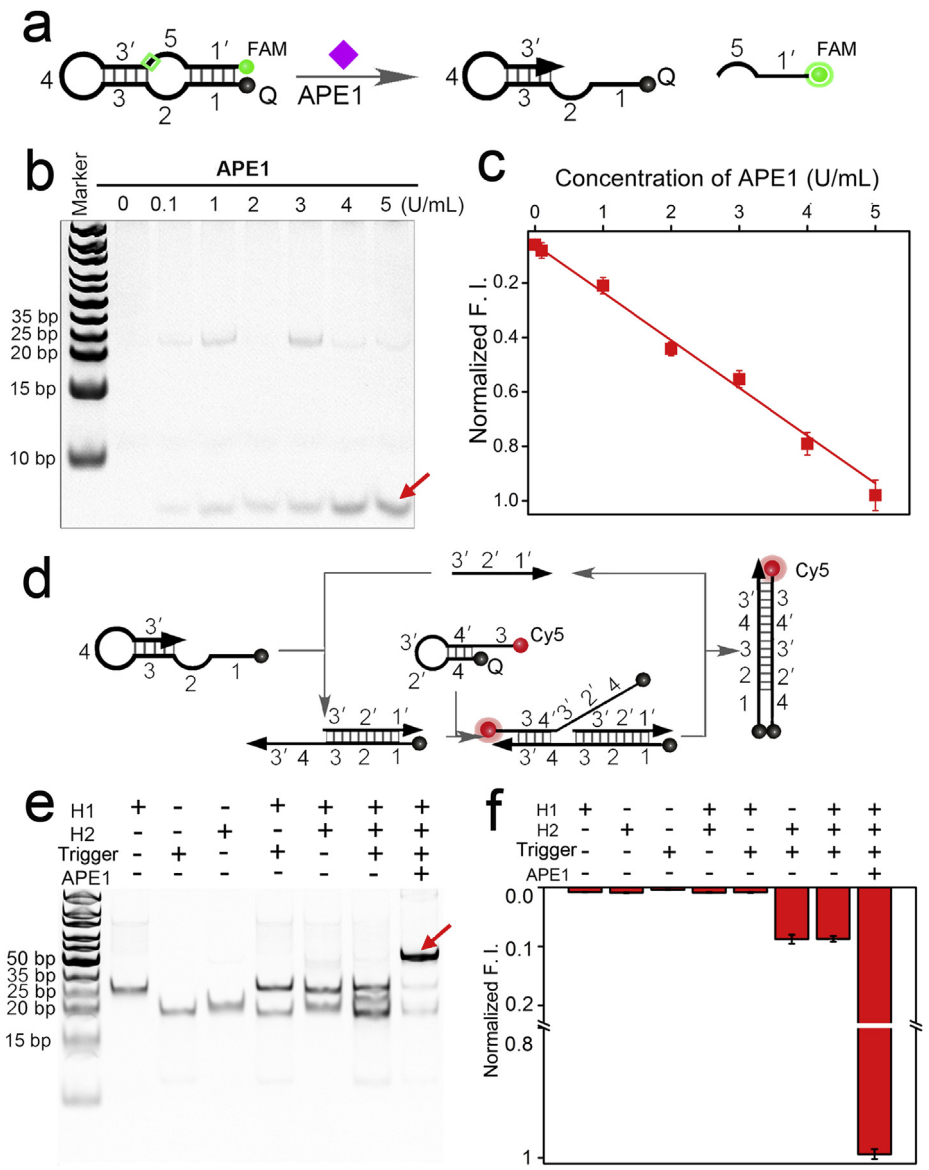

Fig. 1. (a) Scheme of fluorophore (FAM)-labeled hairpin I for the measurement of the activity of APE1. (b) Electrophoretic analysis of the hairpin I under the catalysis of different amount of APE1. (c) Fluorescence intensity of the fluorophore-labeled hairpin I *vs*. the concentration of APE1. Ex: 494 nm, Em: 520 nm. (d) Scheme of CHA launched by the cut hairpin I. (e) Characterization of the CHA products using PAGE. (f) Fluorescence responses of the CHA induced by APE1. Ex: 650 nm, Em: 670 nm.

Furthermore, since the signal of CdS is positively correlated with the activity of APE1 and PbS is negatively correlated with the activity of APE1, the regulation of the enzyme activity can be also detected by using the signal ratio of PbS QDs to CdS QDs, which can display the activity of APE1 better.

3.2. DNA catalytic hairpin assembly triggered by APE1 catalysis

The integrated electrochemical detection system is divided into two parts, i.e. DNA probes for enzyme activity analysis and functionalized electrode for immunoassay, and studied separately. For the former, we first studied the enzymatic cleavage efficiency of APE1 for our designed hairpin I containing AP site. Fluorophore-labeled hairpin I is adopted to facilitate electrophoretic analysis and fluorescence measurements. As is shown in Fig. 1b, a DNA fragment with a small molecular weight pointed by red arrow is observed in the presence of APE1, representing the fluorophore-labeled 3′ fragment released by APE1 enzyme cleavage of the AP site. With the concentration of APE1 enzyme increasing from 0 to 5 U/mL, the brightness of the fluorophore-labeled 3′ fragment strip that is cleaved by the enzyme also gradually increases, suggesting a concentration-depended manner and laying the foundation for quantitative analysis. The results are also confirmed by fluorescence measurements (Fig. 1c).

Next, we studied the feasibility of CHA catalysis by APE1 in the system. As is shown in Fig. 1e, electrophoretic pattern shows that only in the presence of APE1, an expected band of I/II hybrid can be observed, which means only the hairpin I is cleaved by the APE1, and then the 5′ single-stranded DNA of hairpin I is exposed as a toehold to trigger the CHA. In order to accurately verify the occurrence of CHA, fluorophore-labeled hairpin II is also adopted for fluorescence measurements. At the beginning, the fluorescence of the fluorophore Cy5 is quenched by the adjacent quencher BHQ1 in the case of intact hairpin II. But if I/II hybrid is formed, the stretched strand of hairpin II would make a large distance between the fluorophore and the quencher, producing a recovered fluorescence signal. As is expected, Fig. 1f shows that only in the presence of APE1, the recovered fluorescence signal is

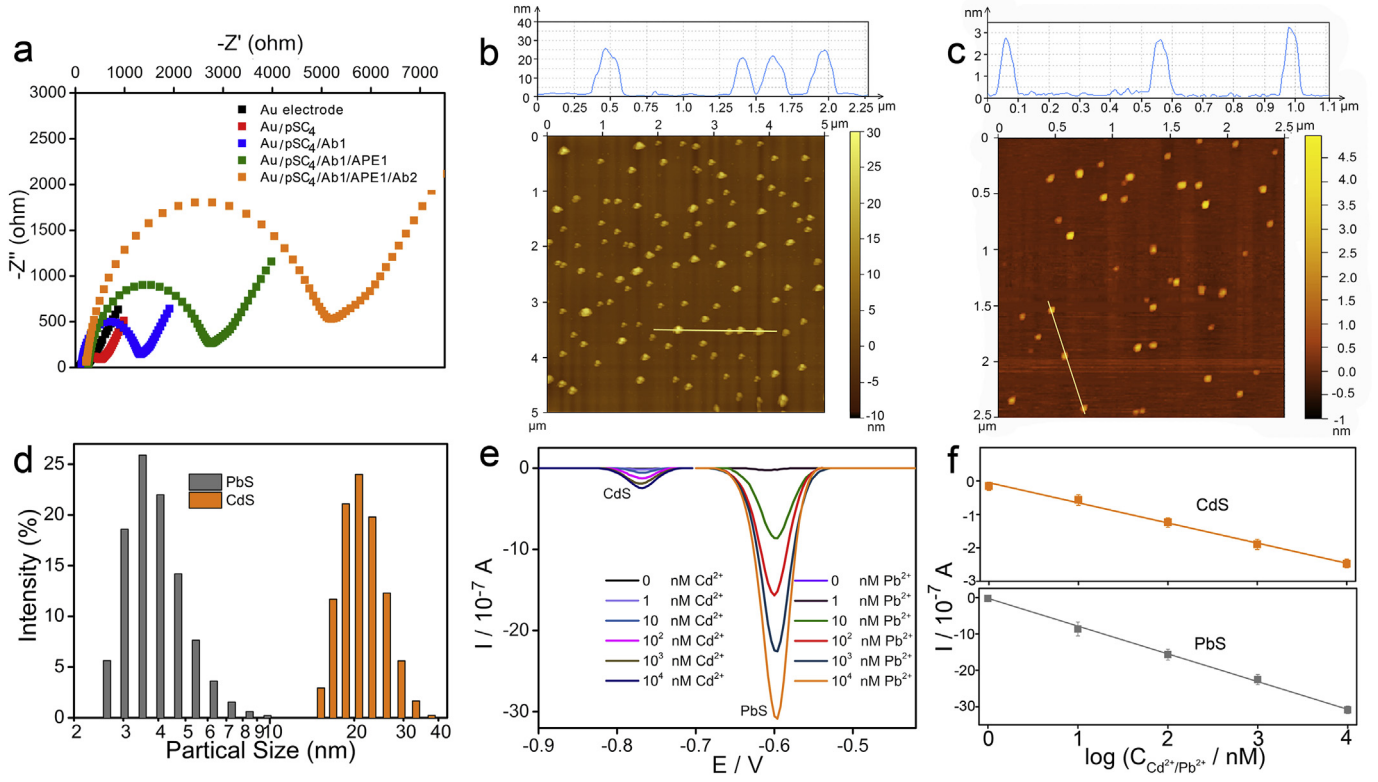

Fig. 2. (a) Electrochemical impedance spectra of the modified electrode. (b) AFM image of CdS QDs. (c) AFM image of PbS QDs. (d) DLS analysis of CdS QDs and PbS QDs. (e) Square-wave voltammograms of CdS QDs and PbS QDs. (f) Linear relationship between the peak currents and the concentration of the QDs. The peak currents were obtained at −0.77 V and −0.6 V for CdS QDs and PbS QDs respectively.

observed. Both electrophoretic and fluorescence results also show that each of the components of CHA, including the hairpin I, the hairpin II, and the trigger chain, is essential for the CHA reaction. The above results together suggest that the enzyme activity of APE1 is able to trigger CHA.

3.3. Characterization of the immuno-functionalized electrode and electrochemical probes

The fabrication of the sandwich structure of Ab1-APE1-Ab2 on the electrode is characterized using a conventional electrochemical impedance spectroscopic (EIS) method. The first layer of antibody (Ab1) is conjugated onto the gold electrode through host-guest recognition with pSC_4, which is pre-immobilized onto the bare electrode through an "Au–SO_3" bond. Fig. 2a shows that the impedance increases with the modification of pSC_4 and Ab1 in sequence. The magnitude of increase is also consistent with the respective molecular weights. In detail, the EIS of bare gold electrode is similar to a straight line. After the immobilization of pSC_4, low molecular weight pSC_4 combining with gold electrode induces a small impedance increase of 50 Ω. Next the high molecular weight protein Ab1 was modified to the gold electrode by the host-guest recognition with pSC_4, which causes a large impedance increase of 1050 Ω. Then, assembly of APE1 and Ab2 by immunological recognition onto the gold electrode causes a dramatic impedance increase to 1500 Ω and 2750 Ω. So, the electrochemical impedance spectra (EIS) results suggest that an immuno-functionalized electrode has been successfully prepared. Moreover, we also use cyclic voltammetry to characterize the assembly process on the electrode, the results of which are consistent with EIS (Fig. S1).

Electrochemically active quantum dots are synthesized and adopted as the electrochemical probes. Atomic force microscope (AFM), dynamic light scattering (DLS) and X-ray photoelectron spectroscopy (XPS) are applied to study the morphology, size distribution and elemental composition of the nanoprobes. As is shown in Fig. 2b–c, spherical CdS QDs and PbS QDs with good dispersity and uniformity can be observed. The diameters of each of them are 20 nm and 3 nm, respectively. DLS results show that both of the nanoprobes have good size distribution (Fig. 2d). The hydrodynamic diameters of each of them are 22 nm and 4 nm respectively, which are consistent with the results of AFM. The existence of Pb, S elements in PbS and the existence of Cd, S elements in CdS were confirmed from the XPS results shown in Fig. S2. Electrochemical responses of these two nanoprobes are also studied using ASV (Fig. 2e–f). Results show that sharp peaks characterizing the oxidation of CdS QDs and PbS QDs can be observed at −0.77 V and −0.6 V respectively. There is a linear relationship between the peak currents and the concentrations of the nanoprobes, laying the foundation for quantitative analysis. It is also noted that the peak positions of these two nanoprobes are significantly separated, which will contribute to dual-signal analysis.

3.4. Integration of the biosensing system for the detection of active APE1

After the study of the two parts of the biosensing system separately, they are ready to be integrated into a whole system and applied for APE1 detection. As is shown in Fig. 3a, in the absence of APE1, no apparent signals can be observed. With the increase of the concentration of APE1, the signals of both CdS QDs and PbS QDs appear. In this case with low concentration of APE1, the enzyme activity of APE1 is not sufficient to catalyze the degradation of all the hairpin I, resulting in the coexistence of CdS QDs-labeled intact hairpin I and PbS QDs-labeled I/II hybrid. It is also noticed that there is positive relationship between the current response of PbS QDs and the concentration of APE1. The result is reasonable, because the more APE1 there is, the more assembled Ab1-APE1-Ab2 and PbS QDs-labeled I/II hybrid will be produced. Both of them contribute to the outputting of the signals of PbS QDs. Also benefited from the amplification of CHA, sensitive detection

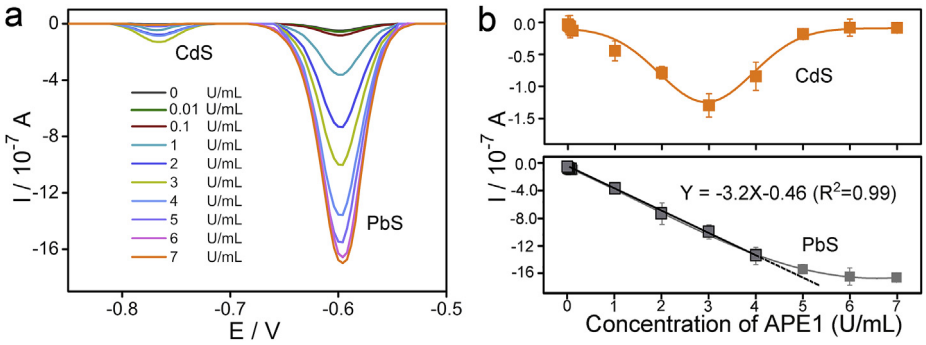

Fig. 3. (a) Square-wave voltammetric signals of CdS QDs and PbS QDs for the detection of APE1. (b) Current responses of CdS QDs and PbS QDs *vs*. the concentration of APE1. The peak currents were obtained at −0.77 V and −0.6 V for CdS QDs and PbS QDs respectively.

of active APE1 using the signals of PbS QDs is achieved. As is shown in Fig. 3b, the detection limit is 0.00518 U/mL, and the linear range is 0.01–4 U/mL. As for the signals of CdS QDs, with the increase of the concentration of APE1, there is a trend from rising to decline. The result should be owing to the antagonism between the positive role of the assembly of Ab1-APE1-Ab2 on the CdS signal and the negative role of the consumption of the CdS QDs-labeled intact hairpin I during the APE1 catalysis. When the APE1 concentration is low, CHA proceeds only slightly, remaining CdS prior to PdS to be assembled onto the electrode. In the meanwhile, the immuno-assembly of APE1 increases sharply with its concentration. These two aspects together cause a rise in the signal of CdS. In the case of a high concentration of APE1, otherwise, CHA converts the signal from CdS to PdS. And in the meanwhile, the immuno-assembly of APE1 tends to saturate. These two aspects together cause a decline after rising in the signal of CdS.

3.5. Comparison with conventional detection methods

We first compare our method with conventional enzyme activity analysis using fluorescent DNA probes (FAM-Probe) (Fang et al., 2015). As is shown in Fig. 4b, the enzyme activity of APE1 can be also detected using the conventional method. The detection limit is 0.028 U/mL, and the linear range is 0.1–5 U/mL. Because of lacking signal amplification, the sensitivity is not as good as our method. Regulation of the enzyme activity by an inhibitor CRT0044876 is also studied. It is observed from Fig. 4c–d, both the conventional method and our method are available for the monitoring of the inhibitor-induced decrease of enzyme activity. The IC_{50} calculated by the two methods are consistent with each other. Endonuclease IV, an isozyme of APE1, is further adopted to study the specificity of the methods. As is expected, endonuclease IV shows fluorescent signals comparable to APE1 by using conventional enzyme activity analysis (Fig. 4e). That is, conventional method cannot discriminate APE1 from its isozyme. But, by using our method, no detectable signals of endonuclease IV can be observed (Fig. 4f). The result is reasonable, since that the immune component of our biosensing system is able to exclude those proteins that cannot be immunologically recognized. This advantage of our method will contribute to the accurate analysis of APE1 in complex physiological samples, e.g. serum and cell extract. So next, we used our method to detect APE1 in three kinds of cells including L02, HeLa and A549 cells (Fig. S3). It was found that the content of enzymatically active APE1 in tumor cells (HeLa and A549) was significantly higher than that of normal cells (L02), and the results were consistent with the literature reports to a certain degree (Zhang et al., 2019).

Next, we compare our method with ELISA, a conventional immunoassay method (Wei et al., 2017). As is shown in Fig. 5a, quantitative detection of APE1 by using a commercially available ELISA kit is achieved. The linear range and the detection limit are 0.01–0.07 U/mL and 0.0023 U/mL respectively, which are comparable to our method. In the presence of the inhibitor CRT0044876, it is observed from Fig. 5b that the signal of APE1 obtained from ELISA barely changes. This result suggests that the immunoassay is not sensitive to the inhibitor-induced structure changes of APE1. Therefore, the regulation of the enzyme activity by the inhibitor cannot be indirectly characterized by ELISA through structural changes, and certainly cannot be directly characterized by ELISA through the changes of enzyme activity. As for the detection specificity, well discrimination of APE1 from its isozyme endonuclease IV can be achieved using ELISA, since endonuclease IV cannot be immunologically recognized by the anti-APE1 antibody. To make a summary of this section, our biosensing method takes into account both immunoassay and enzyme activity analysis, whereas conventional methods can only consider one aspect (Fig. 5d).

4. Conclusions

In summary, we develop a novel electrochemical biosensing system for the detection of APE1. It skillfully integrates immunoassay with enzyme activity analysis through an elaborate design. In this system, once the APE1 is captured onto the electrode through immunological recognition, the DNA-labeled antibody will further recruit the products of CHA triggered by APE1 catalysis, producing amplified signals. Dual-signal, including an “on” signal from PbS QDs and an “off” signal from CdS QDs, is also introduced to ensure the accuracy of the analysis. In this way, both immunoassay and enzyme activity analysis can be achieved by using this integrated biosensing system. A favorable detection performance is thereby obtained. The linear range is 0.01–4 U/mL, and the detection limit is 0.00518 U/mL, both of which are comparable to or better than conventional methods. By optimizing the modification density and the orientation of the antibody on electrode, or adopting other nucleic acid amplification techniques with higher efficiency, it is expected to further increase the detection performance on sensitivity. In addition, monitoring of the regulation of the enzyme activity by an inhibitor and discrimination of APE1 from its isozyme can be both achieved, whereas conventional methods can only consider one aspect. This approach provides a new insight for the analysis of APE1 and opens up new possibilities for the integrated analysis of other kinds of enzymes.

Declaration of competing interest

The authors declare that they have no known competing financial interests or personal relationships that could have appeared to influence the work reported in this paper.

Conflict of interest statement

Mengru Zhou and other co-authors have no conflict of interest.

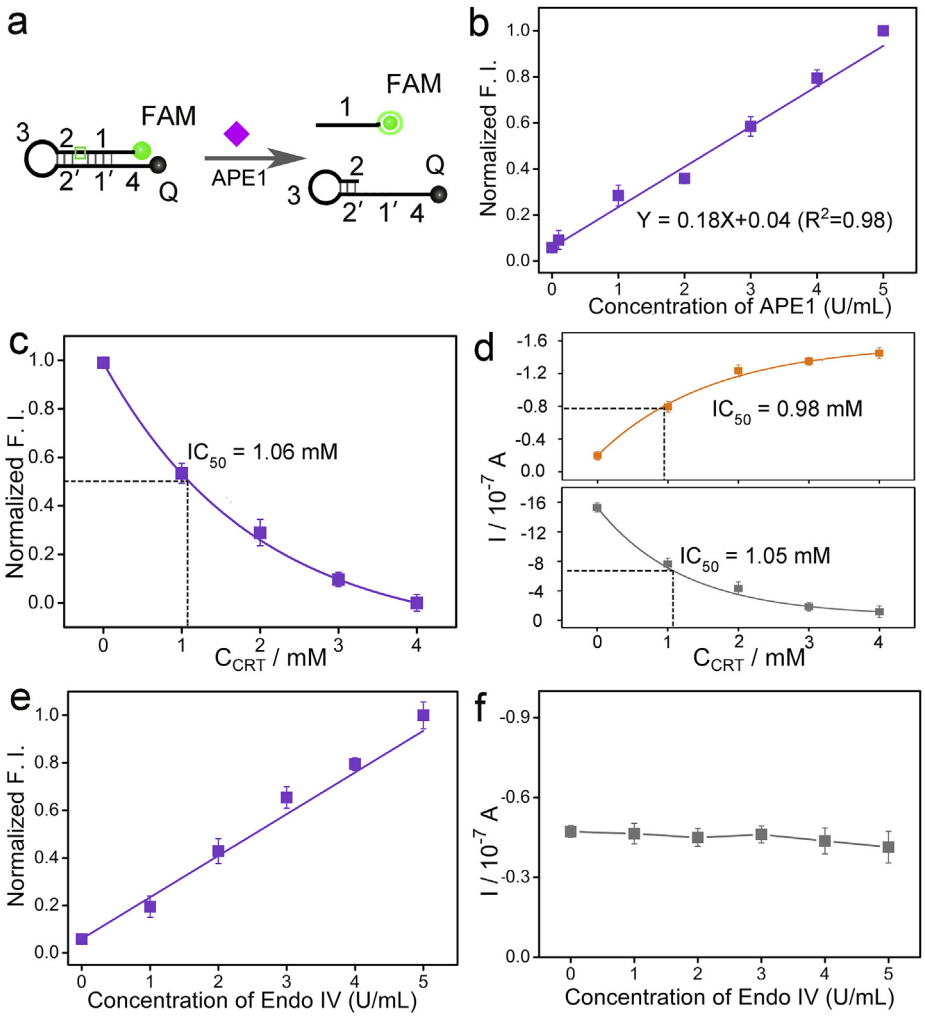

Fig. 4. (a) Scheme of conventional APE1 activity analysis using a fluorescent DNA probe (FAM-Probe). (b) Linear relationship between the relative fluorescence intensity and the activity of APE1. Ex: 494 nm, Em: 520 nm. (c) Changes of the relative fluorescence intensity caused by different concentrations of the inhibitor CRT0044876 using the conventional fluorescent DNA probe-based method. Ex: 494 nm, Em: 520 nm. (d) Changes of the current response of CdS QDs and PdS QDs caused by the inhibitor using our electrochemical method. (e) Linear relationship between the relative fluorescence intensity and the activity of Endo IV using the conventional fluorescent DNA probe-based method. (f) Current response of PdS QDs in the presence of different concentrations of Endo IV using our method.

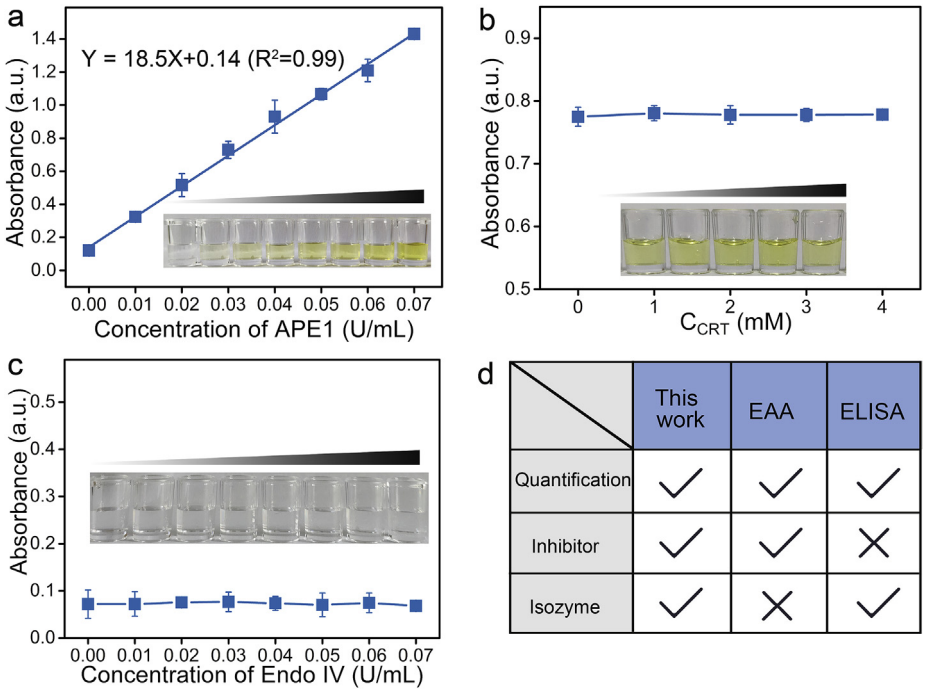

Fig. 5. (a) UV–Vis absorption characterization of ELISA method for detecting APE1. (b) Effect of inhibitor CRT0044876 on ELISA detection of APE1. (c) UV–Vis absorption of the APE1 ELISA kit for the detection of Endo IV. (d) A table summarizing the comparison among fluorescence, ELISA and our electrochemical method.

CRediT authorship contribution statement

Mengru Zhou: Conceptualization. **Chang Feng:** Conceptualization. **Dongsheng Mao:** Data curation, Formal analysis. **Shiqi Yang:** Data curation, Formal analysis. **Lingjie Ren:** Data curation, Formal analysis. **Guifang Chen:** Writing - original draft. **Xiaoli Zhu:** Writing - review & editing.

Acknowledgment

This work was supported by the National Natural Science Foundation of China (Grant Nos. 21575088, 81873539) and the Natural Science Foundation of Shanghai (19ZR1474200).

Appendix A. Supplementary data

Supplementary data to this article can be found online at https://doi.org/10.1016/j.bios.2019.111558.

References

Antoniali, G., Serra, F., Lirussi, L., Tanaka, M., D'Ambrosio, C., Zhang, S., Radovic, S., Dalla, E., Ciani, Y., Scaloni, A., Li, M., Piazza, S., Tell, G., 2017. Nat. Commun. 8, 1–18.
Chaim, I.A., Nagel, Z.D., Jordan, J.J., Mazzucato, P., Ngo, L.P., Samson, L.D., 2017. Proc. Natl. Acad. Sci. U. S. A 114, 10379–10388.
Chang, I.Y., Kim, J.N., Maeng, Y.H., Yoon, S.P., 2013. Redox Rep. 18, 165–173.
Chen, H., Huang, J., Lee, J., Hwang, S., Koh, K., 2010. Sens. Actuators B Chem. 147, 548–553.
Demple, B., Sung, J.S., 2005. DNA Repair 4, 1442–1449.
Dong, H., Zou, F., Hu, X., Zhu, H., Koh, K., Chen, H., 2018. Biosens. Bioelectron. 117, 605–612.
Fang, S., Chen, L., Zhao, M., 2015. Anal. Chim. Acta 812, 168–175.
Gerhard, Fritz, Bernd, Kaina, 1999. Oncogene 18, 1033–1040.
Gines, G., Saint-Pierre, C., Gasparutto, D., 2014. J. Biol. Chem. 288, 8445–8455.
Han, J., Zhuo, Y., Chai, Y., Xiang, Y., Yuan, R., Yuan, Y., Liao, N., 2013. Biosens. Bioelectron. 41, 116–122.
He, C., Wang, M., Sun, X., Zhu, Y., Zhou, X., Xiao, S., Zhang, Q., Liu, F., Yu, Y., Liang, H., Zou, G., 2019. Biosens. Bioelectron. 129, 50–57.
Hegde, M.L., Hazra, T.K., Mitra, S., 2008. Cell Res. 18, 27–47.
Hegde, M.L., Mantha, A.K., Hazra, T.K., Bhakat, K.K., Mitra, S., Szczesny, B., 2012. Mech. Ageing Dev. 133, 157–168.
Huang, E., Zhou, F., Deng, L., 2000. Langmuir 16, 3272–3280.
Katarzyna, Bebenek, Agnès, Tissier, Ekaterina, G. Frank, John, P. McDonald, Rajendra, Prasad, Samuel, H. Wilson, Roger, Woodgate, Thomas, A. Kunkel, 2001. Science 291, 2156–2159.
Lipton, A.S., Heck, R.W., Primak, S., McNeill, D.R., Wilson, D.M., Ellis, P.D., 2008. J. Am. Chem. Soc. 130, 9332–9341.
Lee, Y., Lee, E.K., Cho, Y.W., Matsui, T., Kang, I.-C., Kim, T.-S., Han, M.H., 2003. Proteomics 3, 2289–2304.
Li, J., Yin, T., Qin, W., 2015. Anal. Chim. Acta 876, 49–54.
Li, T., Fan, Q., Liu, T., Zhu, X., Zhao, J., Li, G., 2010. Biosens. Bioelectron. 25, 2686–2689.
Li, Y., Gabriele, E., Samain, F., Favalli, N., Sladojevich, F., Scheuermann, J., Neri, D., 2016. ACS Comb. Sci. 18, 438–443.
McKenzie, J.R., Zhang, C., Li, C.Z., 2013. Electroanalysis 25, 341–344.
Pascut, D., Sukowati, C.H.C., Antoniali, G., Mangiapane, G., Burra, S., Mascaretti, L.G., Buonocore, M.R., Crocè, L.S., Tiribelli, C., Tell, G., 2019. Oncotarget 10, 383–394.
Qin, X., Wang, L., Xie, Q., 2016. Sensors 16, 1342.
Shin, J.H., Choi, S., Lee, Y.R., Park, M.S., Na, Y.G., Irani, K., Lee, S.D., Park, J.B., Kim, J.M., Lim, J.S., Jeon, B.H., 2015. Cancer Res. Treat. 47, 823–833.
Sutter, J., Lindner, E., Gyurcsanyi, R.E., Pretsch, E., 2004. Anal. Bioanal. Chem. 380, 7–14.
Tsutakawa, S.E., Shin, D.S., Mol, C.D., Izumi, T., Arvai, A.S., Mantha, A.K., Szczesny, B., Ivanov, I.N., Hosfield, D.J., Maiti, B., Pique, M.E., Frankel, K.A., Hitomi, K., Cunningham, R.P., Mitra, S., Tainer, J.A., 2013. J. Biol. Chem. 288, 8445–8455.
Wang, L.J., Luo, M.L., Yang, X.Y., Li, X.F., Wu, Y., Zhang, C.Y., 2019. Theranostics 9, 4450–4460.
Wang, X., Du, D., Dong, H., Song, S., Koh, K., Chen, H., 2018. Biosens. Bioelectron. 99, 375–381.
Wei, X., Li, Y.B., Li, Y., Lin, B.C., Shen, X.M., Cui, R.L., Gu, Y.J., Gao, M., Li, Y.G., Zhang, S., 2017. J. Cancer 8, 1492–1497.
Whitaker, A.M., Flynn, T.S., Freudenthal, B.D., 2018. Nat. Commun. 9, 399.
Xiao, Q., Wu, J., Dang, P., Ju, H., 2018. Anal. Chim. Acta 1032, 130–137.
Zhang, Y., Deng, Y., Wang, C., Li, L., Xu, L., Yu, Y., Su, X., 2019. Chem. Sci. 10, 5959–5966.
Zhao, M., Chai, X.D., Han, J., Gui, G.F., Yuan, R., Zhuo, Y., 2014. Anal. Chim. Acta 846, 36–43.
Zhao, Y., Zhang, J., Wang, X., Chen, B., Xiao, Z., Shi, C., Wei, Z., Hou, X., Wang, Q., Dai, J., 2010. J. Control. Release 141, 30–37.
Zhong, Z., Li, M., Qing, Y., Dai, N., Guan, W., Liang, W., Wang, D., 2014. Analyst 139, 6563–6568.
Zhuo, Y., Liao, N., Chai, Y.Q., Gui, G.F., Zhao, M., Han, J., Xiang, Y., Yuan, R., 2014. Anal. Chem. 86, 1053–1060.